Applied Surface Science 608 (2023) 155232

Contents lists available at ScienceDirect

Applied Surface Science

journal homepage: www.elsevier.com/locate/apsusc

Full length article

On the role of surface charge and surface tension tuned by surfactant in stabilizing bulk nanobubbles

Xiaotong Ma[1], Mingbo Li[*,1], Xuefei Xu, Chao Sun

Center for Combustion Energy, Key laboratory for Thermal Science and Power Engineering of Ministry of Education, Department of Energy and Power Engineering, Tsinghua University, Beijing 100084, China

ARTICLE INFO

Keywords:
Bulk nanobubble
Surfactant
Surface charge
Surface tension
Stability

ABSTRACT

The abnormal stability of bulk nanobubbles has attracted substantial attention from academia and industry since classical Epstein–Plesset theory predicts that gas bubbles cannot keep stable thermodynamic equilibrium spontaneously. The dual nature of ionic surfactants, acting simultaneously as charge carriers and attenuators of surface tension at the gas–liquid interface, enables them to play a unique role in bulk nanobubble stabilization. Herein the stability of bulk nanobubbles in anionic, cationic and nonionic surfactant solutions over a wide range of concentration is studied. Experimental results show that different kinds of surfactant molecules are involved in the nucleation and stabilization of bulk nanobubbles in different ways. We demonstrate that the accumulation of net charges carried by surfactant ions at the interface is predominantly responsible for stabilizing nanobubbles, instead of the reduction of surface tension. With theoretical calculations, we further quantify the coupling action of interfacial tension and surface charge on the stable equilibrium state of bulk nanobubbles. The result illustrates that the interfacial tension and the degree of gas saturation together determine the upper limit of the bubble size that can exist stably. Our study identifies a route to explore the intrinsic mechanism of bulk nanobubble's stability.

1. Introduction

Bulk nanobubbles are nanoscale gaseous domains (less than 1 μm in diameter) freely suspended in a continuum of liquid [1], typically, aqueous solution. Over the last two decades, academic and industrial interests in nanobubbles have been accelerated owing to the anomalous characteristics and huge potential for applications in many fields [2–7]. The bewildering points over nanobubbles stem from the divergence between classical theoretical prediction and experimental observation. According to the wide-accepted Epstein–Plesset model [8], bulk bubbles should be unstable under any case: or dissolve rapidly in low gas supersaturation solutions due to the high Laplace pressure, or grow indefinitely in high gas supersaturation solutions, rise to the free liquid level and eventually collapse. Instead, using the detection techniques such as Light scattering, Darkfield imaging, and Cryo-Transmission Electron Microscopy, many experimental reports claim that the observed bulk nanobubbles can survive for weeks or even months [1,9,10]. Therefore, the most critical question on bulk nanobubbles naturally arises: how an isolated bulk nanobubble maintain the thermodynamic equilibrium state while inhibiting diffusion.

Up to now, several stabilization mechanisms for bulk nanobubbles have been proposed from various perspectives. It is claimed that the bulk nanobubbles can be stabilized by being armored with some kind of contamination that balances the gas influx and outflux dynamically [11], or by the particle coats that exert mechanical stress on the interface to counter the Laplace pressure [12]. This mechanism does not seem to be controversial considering that particle-coated microbubbles have been successfully used as ultrasound contrast agents in medical diagnosis. Nevertheless, the model is applied on the premise that the liquid system must be assumed to dissolve ubiquitous contaminant species, even after rigorous purification. This contradicts existing experiments showing that nanobubbles can survive generally in ultrapure water, and does not explain the size selection of nanobubbles ranging from ~100 to ~500 nm measured by dynamic light scattering technique [13]. It does not work in all cases, at least not yet. Besides, some studies put forward that the ultrahigh gas density [14], unusual surface tension at nanoscales [15,16] or gas–water interface polarization [10] are responsible on the stabilization of bulk nanobubbles. More experimental evidence is needed to back it up.

Recently, it has been conjectured that the long-term presence of bulk nanobubbles is caused by the accumulation of negative charges

* Corresponding author.
E-mail address: mingboli@mail.tsinghua.edu.cn (M. Li).
[1] Xiaotong Ma and Mingbo Li contributed equally to this work.

https://doi.org/10.1016/j.apsusc.2022.155232
Received 10 August 2022; Received in revised form 27 September 2022; Accepted 5 October 2022
Available online 11 October 2022

at the gas–liquid interface, implying a strong electron affinity [17,18]. The persistently supporting existence is the negative zeta potential (typically −15 to −40 mV in neutral pH solution) measured on the bubble surface. The surface charge buildup not only creates an electrostatic pressure acting radially outward, that counteracts the Laplace pressure effects for individual bulk nanobubbles, but also enhances the repulsive interaction between adjacent nanobubbles to prevent coalescence. This idea, known as the charge stabilization mechanism, has been widely discussed and extended recently due to the available experimental results and the compelling theoretical basis [19–22]. This mechanism can provide qualitative explanations for both the thermodynamic equilibrium and colloidal stability of bulk nanobubbles [13]. Quantitative theoretical predictions, however, do not compare well with experiments. The central challenge is twofold: first, the fundamental ambiguity of the measuring location, magnitude, and even the sign of the zeta potential; second, the uncertainty about the physical origin of electric charge at the gas–liquid interface.

Although the origin of nanobubbles' charging interface is still intensely debated [23–27], the unique physicochemical properties of the liquid environment in which they are generated and exist have a great influence on the interface charging process, essentially, the thermodynamic equilibrium state. Among other factors, charge carriers in liquid, such as dissolved ions and surfactants, should be taken into account seriously. Considerable research efforts have been devoted to prove that the concentration of ions at the interface is markedly different from that in bulk, owing to the presence of a dielectric discontinuity and difference of the dielectric constant between the interfacial water and bulk water [28,29]. Our recent work [30] studied the stability of bulk nanobubbles in electrolyte solutions with different pH and ionic strengths, and further explained the surface charging behaviors and sign reversal of the zeta potential. We found that, the enhanced stability with increasing acidity or alkalinity of the aqueous solutions arises from the competing-adsorption interactions of different ions at the air–water interface.

As for surfactant, its classification, according to the charged characteristic of hydrophilic head groups, falls under anionic, cationic, nonionic, and amphoteric. Apart from the amphoteric surfactant, the remaining types of surfactants are ubiquitous in everyday life and play an important role in wide industrial applications [31–33]. Compared to ions, surfactants prefer to gather near the air–water interface owing to the amphiphilic molecular structure, which contains both hydrophobic tail groups and hydrophilic head groups [34]. Especially, once dissolved, the ionic surfactant dissociates into the hydrophobic part with the charged head group and the counterion in water. They not only act as charge carriers to adsorb onto the gas–liquid interface, but also reduce the surface tension, both of which appear to be beneficial for bubble stabilization. It has been proven that the adsorption of amphiphilic molecules (insoluble surfactants) at the interface of microbubbles can achieve a short-term stabilization [35]. If the molecules crystallize on the gas–liquid interface (condensed state), the individual bubbles may survive for a few months. By far there already have been several works devoted to the effects of surfactants on bulk nanobubbles qualitatively [19,36–38], relying on assumption that the surfactants adsorb onto the surface of bulk nanobubbles. However, most of the experiments lack a reasonable and quantitative description of how surfactant molecules are adsorbed to the interface. Particularly, the core problem that how surfactants affect the stabilization of bulk nanobubbles through the coupling interaction between surface charge and surface tension, until now, has not been explicitly solved.

In the present research, we are concerned primarily with a quantitative description of the role of surfactants in nanobubble stabilization via experiments and theory. The bulk nanobubbles are generated respectively in anionic, cationic and nonionic surfactants solutions with different concentrations using ultrasonic cavitation method. The results were applied to evaluate the properties and origin of the bulk nanobubbles stability jointly.

2. Materials and methods

2.1. Materials

Hexadecyltrimethylammonium bromide (CTAB, ≥ 99.0%, GC), Sodium dodecylsulfate (SDS, ≥ 99.0%, GC) and Polysorbate 20 (Tween 20, BioXtra) were purchased from Sigma Aldrich (Germany). The chemical structures of the three kinds of surfactant molecules are shown in Fig. 1(a). After dissolving in aqueous solution, the ionic surfactants (CTAB and SDS) dissociate into the hydrophobic part with the charged head group and the counterions in water. The CTAB dissociates into CTA^+ and Br^-, while the SDS dissociates into DS^- and Na^+. The hydrophobic parts show a propensity to move towards the gas phase while the head groups form a charged layer at the gas–liquid interface. The nonionic surfactant (Tween 20) is always distributed in bulk water in molecular form. Ultrapure water (thereafter referred to as pure water) was obtained by a Millipore water treatment system (Milli-Q, Merck, Germany), presenting a pH of 6.5 at room temperature 25 °C and electrical conductivity of 18.2 MΩ cm. All chemicals were used as received without further purification. The critical micelle concentrations (CMC) of CTAB, SDS and Tween 20 at 25 °C are 0.92 mM, 8.2 mM and 0.06 mM, respectively. In this study, the concentration of these three surfactants dissolved in the aqueous solutions was below the CMC, which means that no micelles form in the solution system. For the purpose of complete dissolution, the surfactant molecules were dissolved in pure water at a certain concentration using a magnetic stirrer for 30 min at 25 °C.

All glassware was immersed in a 10% sodium hydroxide and then cleaned for 30 min using ultrasonication. After rinsing with pure water, the glassware was cleaned by ultrasonically with ethanol (≥ 99.0%, AR, Titan, China) and pure water for at least 30 min. Prior to experiments, purified water was initially examined for any nanoscale impurities using Dynamic light scattering and Nanoparticle tracking analysis techniques, and no significant detectable nanoscale entities were observed.

2.2. Nanobubble generation

The bulk nanobubble samples were produced by the ultrasonic cavitation method, in which a probe-type ultrasonic liquid processor (VCX 750 W model, Sonics & Materials, USA) is equipped. Prior to any experiment, the titanium probe (0.75 inch in diameter) was cleaned with pure water and ethanol with at least 5 min ultrasonic treatment to reduce the possible fall-off contaminants. The probe was then used to irradiate 100 mL surfactant solutions, which were stored in a glass beaker, as depicted in Fig. 1(b). A water recirculating cooler (PolyScience PP15r-40, USA) was used to control the temperature of the sample at 25 °C during the ultrasonic treatment. The ultrasonic time and energy input were varied with experiments. In this study, a pulse mode of 20 s ON & 10 s OFF was adopted. After generation, the nanobubble samples were stored in a 100 mL air-tight glass bottle without any further processing.

According to our previous works [30,39], sonication time is a key factor in the generation of bulk nanobubbles, and substantially influences their number concentration and size distribution. The longer sonication treatment, the greater energy input and the more nucleation sites in liquid created, which leads to higher nanobubble concentration. Besides, the ultrasonic probe may inevitably drops small amounts of nanoscale contaminants, predominantly titanium dioxide, into the solutions that serve as nucleation sites and contribute to the concentration of bulk nanobubbles. However, the amount of these contaminants is very small when the sonication time is not long and the system is cooled in time [9], so we ignore their effects in this study.

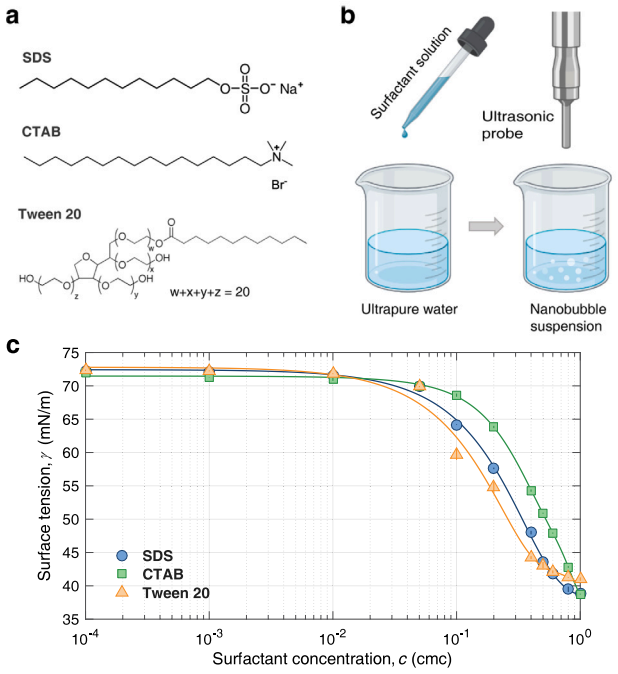

Fig. 1. (a) Structural formulas of anionic surfactant SDS, cationic surfactant CTAB and nonionic surfactant Tween 20. (b) Sketch of the experimental setups for nanobubble generation. (c) Surface tension as a function of surfactant concentration for SDS, CTAB and Tween 20. The solid lines represent the best fit.

2.3. Characterization of nanobubble suspension

Dynamic light scattering (DLS) measurements were carried out using a Zetasizer NanoZSE Instrument (ZEN3700, Malvern Instruments, Malvern, UK) to measure the nanobubble size. In short, a coherent laser was directed into the sample suspension, ensuring the nanobubbles as light scatters could be observed. Photodetectors were employed to record the temporal Brownian motion, recovering a histogram of bubble size. All the measurements were performed at 25 °C using a He–Ne laser (wavelength 633 nm) under the quasi-backscattering configuration (scattering angle 173°).

The zeta potential of bulk nanobubbles was characterized using this instrument as well based on the electrophoretic mobility of charged particles. The electrophoretic mobility was obtained by performing an electrophoresis experiment on about 1 mL sample sealed in a curved capillary U-shape cell. The migration velocity of the bulk nanobubbles was thus measured using the Laser Doppler Velocimetry. The zeta potential was calculated based on the Smoluchowski model. Automatic runs (1∼100) for each sample were performed at least 6 times, and the time interval between each measurement was 10 s. The temperature of all the measurements was set at 25 °C.

Meanwhile, the size distribution and number concentration of these nanobubble suspensions were also detected by the nanoparticle tracking analysis technique (NTA, self-built), which consists of a laser, a microfluidic sample cell, an inverted dark-field microscope equipped with a high-speed camera [30,39]. The nanoparticlas in the sample chamber were illuminated by a laser beam with a wavelength of 520 nm and visualized by an optical microscope (IX73, Olympus, Japan) with a long working distance objective (×20 magnification). A CCD camera was employed to capture the Brownian motion of the illuminated nanoparticles under a framerate of 30 fps. The video captured in random positions were analyzed by ImagesJ/Fiji [40] and NanoTrackJ [41] to obtain the size distribution and number concentration of the nanobubble samples.

2.4. Surface tension measurements

The Surface tension of solution containing different concentrations of surfactant was measured using a surface and interface tensiometer (DCAT25, DataPhysics, Germany). The Wilhelmy plate method was applied. The uncertainty is about ±0.2 mN/m. When the specific plate with known length and height was fixed on the tensiometer and contacted with the gas–liquid interface, a liquid film formed owing to the contribution of surface tension. We measured the surface tension via both the gravitational force of the liquid film and the length of the contact line. The results for these three surfactant solutions were shown in Fig. 1(c) under calibration using pure water and ethanol. For each example, three measurements were performed at a temperature of 25 °C and the average was obtained. The surface tension decreases from the typical value of pure water (72 mN/m) with the increasing concentration of surfactants until the CMC.

3. Results and discussion

3.1. Effect of surfactant on bulk nanobubble nucleation

In our previous works [30,39], we have compared the results obtained by DLS (intensity-weighted) and NTA (number-weighted) techniques for nanobubble size detection. Similarly, both techniques are used in this study. Although DLS can detect nanoparticle sizes down to 0.4 nm, the resolution limit of NTA technique (on the order of ∼10 nm) is enough for this study. Considering the heterogeneous feature of the bulk nanobubble size distribution, the presented results on nanobubble size thereinafter are mainly measured by NTA technique.

In addition, it should be noted that cavitation erosion occurs when the ultrasonic power reaches 750 W. There would be nanoparticles during the ultrasonication, which are mainly released from the ultrasonic probe. The formation and stability of bulk nanobubbles are influenced by the presence of nanoparticles [42]. It has been reported that the nanoparticles in solution provide nucleation sites and promote bulk nanobubbles generation, leading to an enhancement in bubble number concentration [43,44]. Some researchers [45] discover that bulk nanobubbles suspension interacts with new nucleation on the nanoparticles, which is different from froth flotation, where bubble–particle interactions are driven mainly through collisions. The formation of one-particle-one-bubble agglomerations contributes to the colloidal stability of suspensions. In addition, previous research [46] has claimed that bulk nanobubbles are armored by a solid coating made up of self-assembly nanoparticles at the interface of shrinking bubbles. The shell appears to stabilize the bulk nanobubbles by providing mechanical resistance to huge Laplace pressure. However, much of the work reported is lack in-situ detection owing to the limitation of the technique, and further demonstrations are necessary to verify the intrinsic interactions between nanobubbles and nanoparticles. In other words, it is a complicated and open question [42]. In the experiments, it is inevitable to produce nanoparticles along with the formation of bulk nanobubbles during ultrasonic cavitation. Nevertheless, the amount of these nanoparticles produced by the ultrasonic cavitation method is very low based on freezing-thawing experiments and inductive coupled plasma-mass spectrometry measurements [9,47]. In this work, we focus on the effects of surfactants on the characteristics and stability of bulk nanobubbles, and overlook the impacts of shed nanoparticles.

The size distributions of bulk nanobubbles generated in different types of surfactant solutions are shown in Fig. 2. The surfactants, spanning several orders of magnitude concentrations (10^{-4} ∼ 1 cmc), were added before ultrasonic cavitation treatment. The results show that, bulk nanobubbles do actually nucleate and survive in any surfactant environment, with a similar range of size distributions (<∼500 nm in diameter) and an almost consistent characteristic peak centered at ∼125 nm. However, compared with the other two, the size distribution range of nanobubbles generated in SDS solutions is narrower

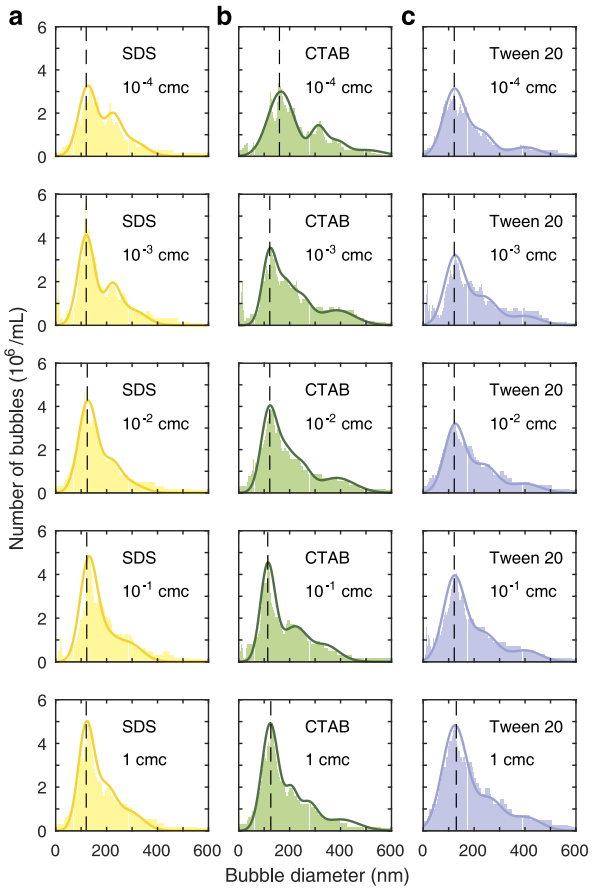

Fig. 2. Size distribution of bulk nanobubbles generated at various concentrations of (a) anionic surfactant (SDS), (b) cationic surfactant (CTAB) and (c) nonionic surfactant (Tween 20). The dashed lines mark the peak size.

(<~400 nm typically). Large nanobubbles seem to disappear or do not nucleate initially under the influence of anionic surfactants. For the three cases, as the surfactant concentration increases, the bubble size distribution becomes more concentrated with a more pronounced peak. The monodisperse size distribution of nanobubbles largely reduces the Ostwald ripening effect, in which large bubbles grow by consuming smaller neighboring ones [48,49]. When nanobubbles of different sizes coalesce, the size of the bubble will continue to increase until large enough to escape from the liquid directly. Therefore, the monodisperse size distribution contributes to the stability of bulk nanobubbles to some extent.

In addition, the internal gas type plays an important role in the nucleation and stability of bulk nanobubbles. The generation of bulk nanobubbles is determined not only by the number of dissolved gas molecules but also by the type of gas. The nucleation threshold depends on the specific interactions between gas molecules and water molecules [50]. It has been reported that dissolving gas molecules with high polarizability in water could increase the number of bubbles produced by cavitation, due to the reinforced interactions between gas molecules and water molecules. Besides, some studies have systematically investigated that gas type influences the properties of nanobubbles, including size distribution, number concentration, zeta potential, and long-term stability [51,52]. However, the experimental results are scattered due to the diversity of experimental conditions and the limitations of experimental techniques. In this work, the bulk nanobubbles are generated by the ultrasonic cavitation method. The surfactant solutions stored in an open glass beaker are treated with an ultrasonic probe. After generation, bulk nanobubbles suspensions are conserved in the airtight glass without any further processing. No other extra gas is introduced throughout the ultrasonic cavitation and preservation process. In our opinion, the main component of gas inside the nanobubble is the mixture of oxygen, nitrogen, carbon dioxide and vapor. However, it is hard to confirm the content of bulk nanobubbles due to a lack of in-situ measurements. Leveraging advanced tools to measure the component of bulk nanobubbles is likely to further improve our understanding of the stabilization mechanism.

Next, we explore the effect of surfactants (SDS, CTAB, and Tween 20) on nanobubble nucleation based on the bubble number density (concentration) N_b, mean diameter d_b and zeta potential ζ, as shown in Fig. 3. Diverse behaviors were observed given the rather different chemical nature of these surfactants. As a control, the properties of nanobubbles generated in pure water are first characterized (see Fig. 3(a-1~a-3)), with N_b =~ 1.6 × 10^8/mL, d_b =~ 200 nm, and ζ =~ −10 mV. For the cases of SDS and Tween 20, the presence of surfactants appears to cause a rise in bubble concentration. When the surfactant concentration is low (<~ 10^{-1} cmc), however, changing it has no or little effect on the nanobubble concentration. As for CTAB, an evident decrease in N_b from the value obtained from pure water was observed when CTAB is added in small amounts (<~ 10^{-4} cmc). N_b drops by nearly 20% as the CTAB concentration is increased to about 10^{-5} cmc. This curve displays a nadir, as indicated by the dashed line, after which the N_b increases with CTAB concentration steadily. Interestingly, we note that, when the concentration of added surfactants is 1 cmc, the N_b of all three cases reach an approximately identical maximum of about 1.8×10^8 /mL. Regardless of the type of surfactant, however, their effect on mean bubble diameter d_b is not significant (within ±10%) in the investigated range, as illustrated in the second column of Fig. 3. For the case SDS, the d_b decreases slightly with increasing SDS concentration, while for the case Tween 20, d_b maintains constant at all surfactant concentration levels, which are also observed in previously published work [19]. However, we found that, for the case CTAB, the surfactant concentration dependence of d_b is non-monotonic, which is completely opposite to the trend of N_b, as shown in Fig. 3(a-2). d_b increases firstly and then keeps slightly decreasing. Although the largest mean value (~218 nm) was less than 10% higher, we should emphasize here that these values are time-sensitive as a consequence of the varying stability of these nanobubble samples. These measurements in Fig. 3(a-2) were taken right after the nanobubbles were generated. This trend would become more pronounced over time, which is what we will focus on from the perspective of long-term stability analysis in the next section.

For Zeta potential measurements, the experimental results show more complicated scenarios. For SDS case, the magnitude of ζ increases from −10 mV to −80 mV at elevated surfactant concentration, and levels off above about 0.5 cmc. This promotion can be ascribed to the higher adsorption ratio of SDS molecule on the surface with its hydrophilic ionic head group orientating themselves towards the liquid and the hydrophobic tail towards the gas phase. Above a certain concentration (~0.5 cmc), zeta potential remains unchanged, which might be on account for the limitation of adsorption sites on the gas–liquid surface. Therefore, it is expected that, a saturated level of SDS has been reached, and adsorption and desorption maintain a dynamic equilibrium on the surface. In Fig. 3(a-3), the trend is different remarkably, with a sign reversal due to the presence of positive charges dissociated by cationic surfactant CTAB. On the existence of tiny amounts of CTAB (~ 6×10^{-6} cmc) in the bulk, ζ is close to zero, namely, the isoelectric point (IEP), demonstrating that these nanobubbles are almost uncharged. Above IEP, ζ rises quickly from 0 to approximately 70 mV with increasing CTAB concentration. Here even when the CMC of CTAB is reached, the saturation level of the bubble surface has not been observed. This difference between the CTAB- and SDS-stabilized nanobubbles is attributed to the physicochemical properties of the surfactants, such as size, CMC value and surface activity. At IEP, the nanobubble example presents the minimum number density and the maximum mean bubble diameter. The change in Zeta potential is

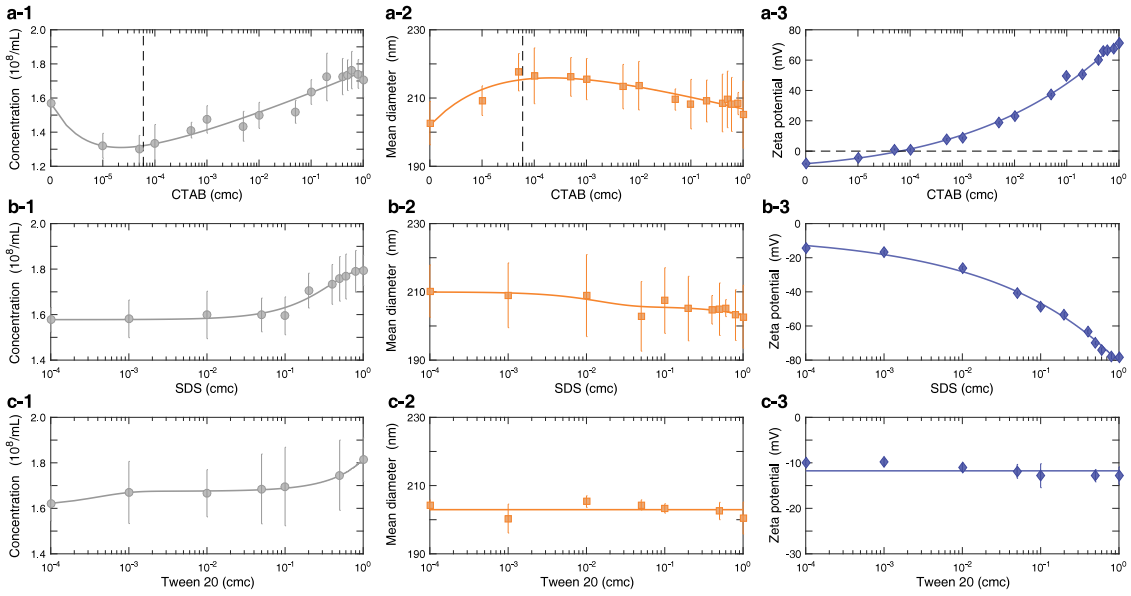

Fig. 3. Effect of surfactant on total number concentration N_b, mean diameter d_b and Zeta potential ζ of bulk nanobubbles generated in (a) cationic surfactant (CTAB), (b) anionic surfactant (SDS), and (c) nonionic surfactant (Tween 20) solutions. In (a-1∼a-3) the experimental results of bulk nanobubbles generated in pure water are added as a control.

attributed to the adsorption of the hydrophilic charged head group at the interface that neutralizes the pre-absorbed negative charges. Since no extra ions are introduced into the solutions, the zeta potential does not change obviously for the case of Tween 20, as shown in Fig. 3(c-3).

Comparing the experimental results of these three cases, we conjecture that, the contributions of surfactants to the change of nucleation rate of bulk nanobubbles originated from two aspects. Firstly, reducing the surface tension of the solution results in the gradual decrease of nucleation threshold [53]. More bubbles can nucleate with the input of ultrasonic energy. Secondly, the high magnitude of Zeta potential (negative or positive) at the bubble surface creates a sufficiently high repulsive force between the adjacent bubbles, that the coalescence between them is effectively suppressed, even with the participation of the Bjerknes force.

3.2. Effect of ionic surfactant on stability of bulk nanobubbles

Apparently, ionic surfactants, whether cationic or anionic, have noteworthy influence on the characteristics of bulk nanobubbles. In particular, the two types of surfactants exhibit excellent agreement in both the reduction of solution surface tension (see Fig. 1(c)) and the enhancement of nanobubble Zeta potential (see Fig. 3(a-3) and (b-3)). So the next question we want to answer is: do the nanobubbles in these two solutions enjoy the same stability? To clarity the stable behavior of nanobubbles, we monitored the time evolution of their properties (size distribution, number density N_b, mean bubble diameter d_b, Zeta potential ζ) over the first 48 h. For SDS and CTAB, two surfactant concentrations, $c_0 = 0.01$ cmc and 0.5 cmc, are selected to better evaluate the coupling effect of surface tension and surface charge. One ($c_0 = 0.01$ cmc) corresponds to high surface tension and low surface potential, while the other ($c_0 = 0.5$ cmc) corresponds to low surface tension and high surface potential. In both cases, the surface tension and the magnitude of Zeta potential caused by the two kinds of ionic surfactants are nearly identical, only with slight deviations.

The experimental data are summarized in Fig. 4. We first show the monitoring results for the low-concentration case (Fig. 4(a∼d)); the high-concentration case is discussed later (Fig. 4(e∼h)). As illustrated in Fig. 4(a), the nanobubbles immersed in the two surfactant solutions exhibit contrasting behaviors: for SDS case the bubble size distribution remains the same even after two days, while for CTAB case the bubble size distribution becomes quite flat, with only a few large bubbles remaining. More quantitatively, the concentration of bulk nanobubbles generated in SDS solution at 0.01 cmc declines slightly within the first 48 h after their generation, as shown in Fig. 4(b). In contrast, however, the concentration of bulk nanobubbles produced in solutions with the same concentration of CTAB surfactant dropped remarkably, with nearly 80% of them disappearing after 48 h. Correspondingly, the mean bubble diameter of nanobubbles in CTAB solution increases observably from ∼ 200 nm to ∼ 350 nm, while that in SDS solution remains constant, as shown in Fig. 4(c). The results regarding the evolution of zeta potential for these two cases are displayed in Fig. 4(d). Both exhibited significant changes, where the zeta potential of the nanobubbles in SDS solution gradually rises from −20 mV to about −50 mV within 48 h. By stark contrast, the zeta potential of the bulk nanobubbles in CTAB solution changes from 20 mV to −10 mV with time. The reversal of the sign of the zeta potential occurs after approximately 24 h. Generally, the charging surface become more and more “negative” with time. After 48 h, regardless of the initial charge sign, the absolute values of both have changed by nearly 30 mV. This also reveals that the reversal of zeta potential on the surface of nanobubbles in CTAB solution is due to the neutralization of the positive charges upon adsorption of negative charges, rather than the desorption of the positive charges. In this regard, there is still enough space on the nanobubble surface to allow the adsorption of the rest of the charged carrier. The accumulation of net interfacial charges decreases, so that the equilibrium condition, whether as a single bubble or as a nanobubble cluster, appears to be destroyed eventually, along with the collapse of individual nanobubbles or coalescence of adjacent nanobubbles. It thus rationalizes the reduced concentration and increased size shown in Fig. 4(b) and (c). These nanobubbles thus are no longer considered a thermodynamic equilibrium phase, even though they can survive for a much longer time than the predictions of classical theory. Hence, these findings indicate that adsorption of surface charges are predominantly responsible of the stability of bulk nanobubbles, instead of surface tension.

If surface charge is the key factor to stabilize bulk nanobubbles, do all the positively charged nanobubbles fail to hold long-term stability? Following the same steps, we monitor the properties of bulk nanobubbles generated in the surfactant solutions with 0.5 cmc SDS or CTAB over a period of 48 h as well, as shown in Fig. 4(e∼h). It can be seen that, there are no remarkable changes in bubble size distribution, number concentration, mean diameter and zeta potential for both. Both the N_b and d_b exhibit a slight decrease over time. This is physically

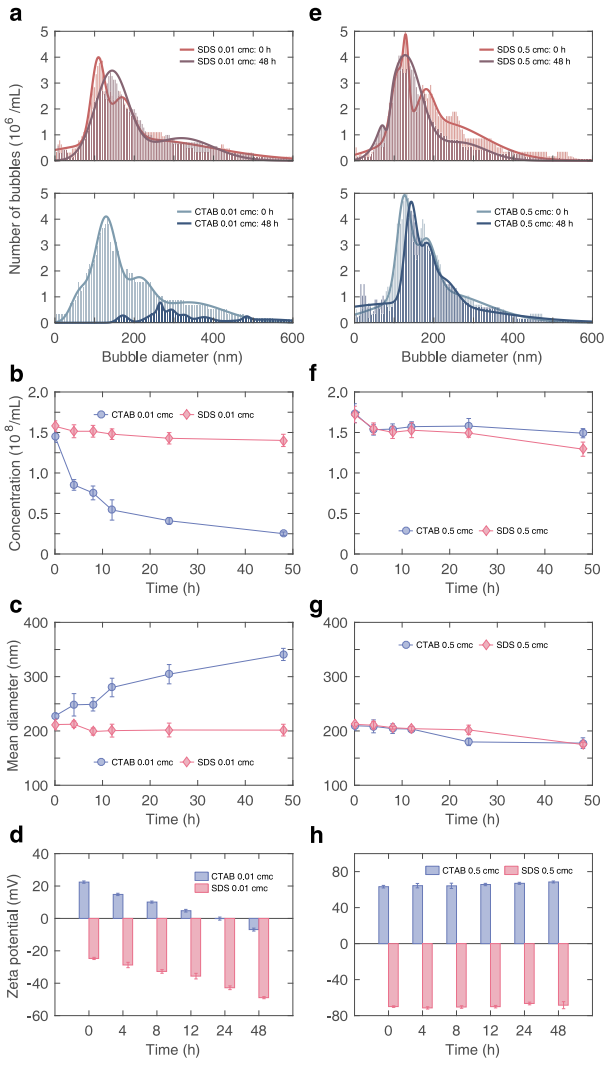

Fig. 4. Bulk nanobubble evolution under ambient conditions and 25 °C after their generation. (a–d) Temporal evolution in size distribution, concentration, mean diameter and Zeta potential over a 48-h period for two nanobubble examples generated and suspended in 0.01 cmc SDS and 0.01 cmc CTAB, respectively. (e–h) Temporal evolution in size distribution, concentration, mean diameter and Zeta potential over a 48-h period for two nanobubble examples generated and suspended in 0.5 cmc SDS and 0.5 cmc CTAB, respectively.

reasonable that what really matters is the amount of surface charges, not their sign and species, which has been demonstrated in our recent work [30]. The high $|\zeta|$ is in favor of achieving a better stability by the electrostatic stress on the bubble surface and electrostatic repulsion between adjacent bubbles. For positively charged nanobubbles, the stability is rapidly restored during the charging process in the solution with a high concentration of CTAB. The positive charges, most probably from the hydrophilic group of CTAB, build up on the nanobubble surface, counteracting the absorption of negative charges. In addition, the reason why little considerable changes occur is the limitation of adsorption sites on the nanobubble surface. In a solution with such a high concentration of ionic surfactant (> 0.5 cmc), the adsorption of surfactant on the bubble surface is sufficient that there are not many vacant sites for the remaining ions in the bulk. It is demonstrated that ionic surfactant is beneficial to the stability of bulk nanobubbles.

Next, a quantitative in-depth analysis of the stability of the bulk nanobubbles that live in different solutions is performed by applying classical DLVO theory [54]. The application of DLVO theory to the systems containing identical nanoparticles is well established. The kinetics stability principally depends on the interplay between two forces: the attractive van der Waals force and the repulsive electrostatic double-layer force. The interaction free energy between charged air/water interfaces of nanobubbles thus can be approximately predicted based on the attractive van der Waals interaction energy E_A and the repulsive electrostatic interaction energy E_R, namely

$$E_T(D) = E_A(D) + E_R(D), \tag{1}$$

where D represents the separation distance between two approaching bubble surfaces. For two spherical bubbles of radii R_1 and R_2 with surfaces D apart ($D \ll R_1, R_2$), the van der Waals component is always negative. Here the electromagnetic retardation effects are taken into account [55] and $E_A(D)$ is given by

$$E_A(D) = -\frac{A}{6D}\frac{R_1 R_2}{R_1 + R_2}\left[1 - \frac{\mathrm{b}D}{\lambda}\ln\left(1 + \frac{\lambda}{\mathrm{b}D}\right)\right], \tag{2}$$

where A is the Hamaker constant, b is roughly equal to 5.32, and λ is the characteristic wavelength of the interaction, generally assumed to be about 100 nm. The Hamaker constant can be calculated from Lifshitz theory [56] if the dielectric properties of the interacting mediums are given over a wide frequency range. In our recent work [30], a full Lifshitz calculation has been well established for air–water–air system by simplifying the expression of A with an effective frequency. Herein the Hamaker constant was taken as $A \approx 7.3 \times 10^{-20}$ J (See Supplemental Material for detailed derivation process).

The electrical double layer repulsive energy E_R can be calculated by the well-known expression

$$E_R(D) = \frac{R_1 R_2}{R_1 + R_2} Z \exp(-\kappa D) \tag{3}$$

in which, for a simple 1:1 monovalent medium solution (as studied in this work), Z is an interaction constant determined by the electrical properties of aqueous solutions and approaching nanobubbles, $Z = 64\pi\epsilon_0\epsilon_w(k_BT/e)^2\tanh^2(ze\psi_0/4k_BT)$, and, κ is the Debye–Hückel parameter $\kappa = \sqrt{(2N_A I e^2)/(\epsilon_w\epsilon_0 k_B T)}$, whose inverse ($\kappa^{-1}$) is the Debye length [54]. Generally, the Debye length indicates the characteristic length-scale at which electrostatic screening interactions reach. In these expressions, $\epsilon_0 = 8.85 \times 10^{-12}$ F/m is the vacuum permittivity, ϵ_w is the relative permittivity of the medium under the given temperature T, k_B is the Boltzmann constant, $e = 1.6 \times 10^{-19}$ C is the electronic charge, z is the ion valency, ψ_0 is the surface potential of bubbles, $N_A = 6.022 \times 10^{23}$ is the Avogadro's number, and I is the ionic strength of the electrolyte expressed in $\mathrm{mol/m^3}$. In previous work [30], we note that when the magnitude of ψ_0 is not very high (< 60 mV), the deviation from the Zeta potential ζ is negligible. Therefore, in the following calculations, the measured ζ in the experiments is regarded as the ψ_0 of bulk nanobubbles.

Considering $R_1 = R_2$, the total interaction energy E_T between two bulk nanobubbles approaching each other was calculated in the presence of different ionic surfactants, as shown in Fig. 5. The E_T is depicted in units of the microscopic thermal energy of the molecules k_BT, and the interspacing distance is normalized with the Debye length κ^{-1}. The total interaction energy profiles in Fig. 5(a) show that, with increasing concentration of ionic surfactant SDS, the energy barrier increases steadily, with a maximum of about 250 k_BT, due to the increase of the electrostatic repulsion. Since the intrinsic potential of bulk nanobubbles in pure water is negative, adsorption of SDS molecules onto the negatively charged surfaces may add more negative charges, thereby increasing the surface charge density. At high concentration the energy barrier is so high that the nanobubbles in dispersion have no chance to gain enough thermal energy to overcome it, and thus enjoy better colloidal stability. The nanobubbles can exist in such a stable state for a sufficiently long time.

However, adding a small amount of CTAB reduces the energy barrier to a certain extent and even induces its disappearance ($E_T \leq 0$), known as the critical coagulation concentration, as shown in Fig. 5(b).

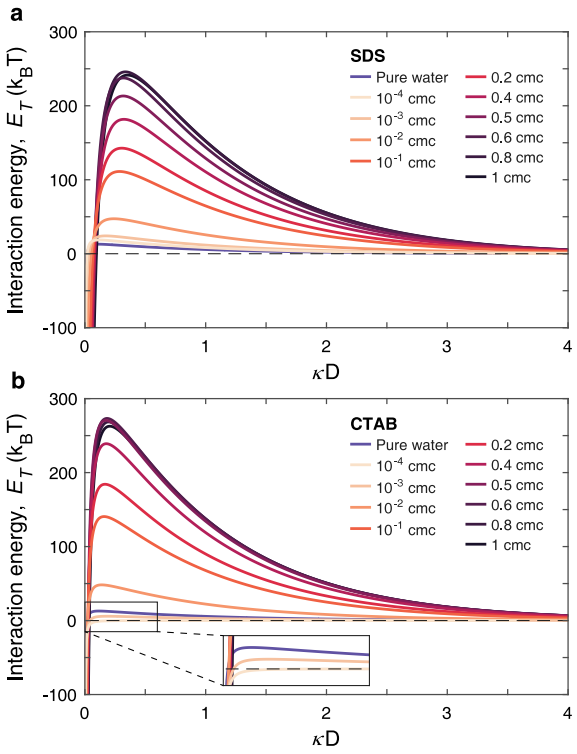

Fig. 5. Total DLVO interaction energy for two interacting bulk nanobubbles as a function of the normalized interspacing distance in the presence of (a) anionic surfactant (SDS) or (b) cationic surfactant (CTAB). Ten different cases are considered depending on the concentration of the surfactant added ranging from 10^{-4} to 1 cmc. Nanobubbles generated in pure water served as controls.

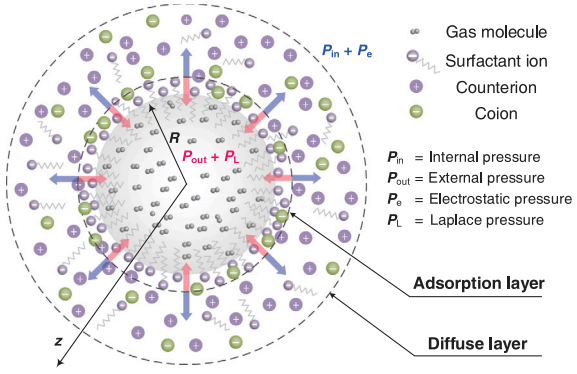

Fig. 6. Schematics of the adsorption layer structure of ionic surfactants surrounding a negatively charged bulk nanobubble. The sharp air–water interface is located at $z = R$ mathematically. Surfactant molecules/ions and counterions around the interface form an adsorption layer of thickness δ, and the diffuse layer starts at $z = R + \delta$.

This discharging process with the subsequent collapse of individual nanobubbles and coalescence between adjacent nanobubbles develops efficiently. Both cause the decay in nanobubble concentration, as shown in Fig. 3(b1). As expected, the bubble–bubble interaction are increasingly dominated by electrostatic interaction energy and the energy barrier appears again as the surfactant concentration is increased from 10^{-3} cmc to 1 cmc. Nevertheless, one should note that the recovery of $E_T > 0$ does not always imply the achievement of nanobubble's long-term stability. The net positive charge accumulated on the nanobubble surface should be sufficient to neutralize the negative charges that are adsorbed continuously from the bulk (see Fig. 4(c)). In other words, the energy barrier should be high enough, at least, greater than 50 k_BT.

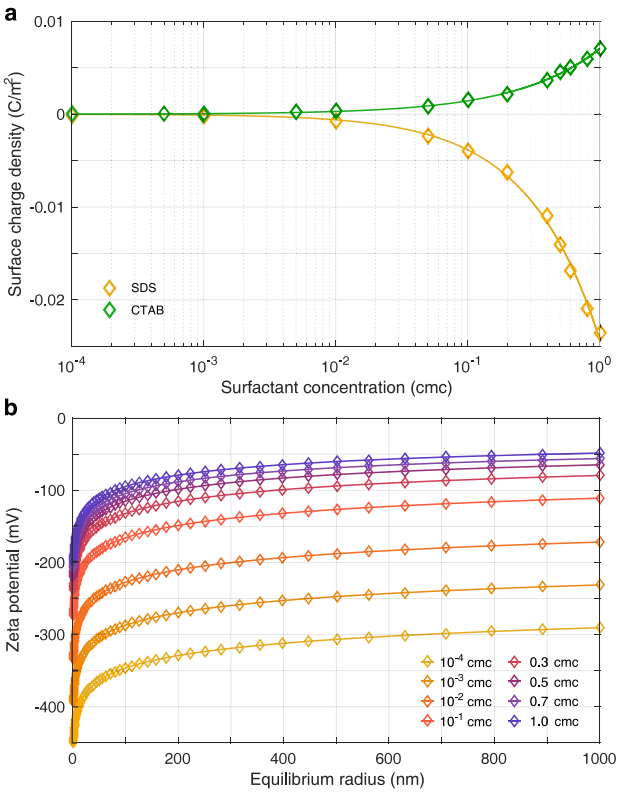

Fig. 7. (a) Surface charge density as a function of the surfactant concentration for SDS and CTAB solutions. The solid lines are power-law fits, e.g., $\sigma \sim c^{0.7/0.8}$. (b) Dependence of the zeta potential on the stable equilibrium radius for nanobubbles generated in various concentrations of surfactant solutions.

3.3. Effect of the dual action of surfactants on the stable equilibrium size of nanobubbles

According to the experimental results, we confirm that the adsorption of surfactants at the interface has notable influences not only on surface tension but also on surface charging, both of which are key factors to maintain the stability of bulk nanobubbles. In order to achieve thermodynamic equilibrium, the individual bubble system should at least be in mechanical (Young–Laplace equation) and chemical (Henry's law) equilibrium (see Fig. 6). Based on the charge-stabilization model [21,22,39], for a single nanobubble it has to obey the following equation:

$$P_{in} + \frac{\sigma^2}{2\epsilon_w\epsilon_0} = P_{out} + \frac{2\gamma}{R}, \tag{4}$$

where P_{in} and P_{out} is the pressure inside and outside the bubbles, respectively. In this study, P_{out} remains constant, i.e., $P_{out} = 10^5$ Pa (atmospheric pressure). According to Henry's law, under a certain temperature, $P_{in} = k_H c_b = k_H c_s(1 + \xi)$, where k_H is the Henry coefficient, c_b is the actual concentration of dissolved gas, c_s is the saturation concentration, and $\xi = c_b/c_s - 1$ is the supersaturation, e.g., $\xi = 0$ corresponds to exactly saturated water. Furthermore, for the spherical electrical double-layer with radius R, the approximate analytical solutions for the surface charge density can be expressed as [57]:

$$\sigma(R) = \frac{2\epsilon_w\epsilon_0 k_B T}{ze\kappa^{-1}} \sinh\left(\frac{ze\zeta}{2k_BT}\right)\left[\frac{1}{\kappa R}\frac{2}{\cosh^2(ze\zeta/4k_BT)} + \frac{1}{(\kappa R)^2}\frac{8\ln[\cosh(ze\zeta/4k_BT)]}{\sinh^2(ze\zeta/2k_BT)} + 1\right]^{1/2}, \tag{5}$$

where z is the valence, e.g., for monovalent 1:1 electrolyte solution, $z = 1$, and the expression in square brackets on the right is a geometric

item derived from the spherical Poisson–Boltzmann equation. It should be noted that the micro-sized bubbles adhere to the thermodynamic equilibrium of bubbles described by the charge stabilization model theoretically. Nevertheless, when the bubble size reaches the micron scale, the buoyancy force on the bubble suspended in the bulk is not negligible. The bubble rises out of the liquid and collapses once its buoyancy $\sim \rho R^4 g$ exceeds the thermal energy $\sim k_B T$. Hence, a threshold radius of around 1 μm of bulk nanobubbles is confirmed by experimental and theoretical perspectives, above which a bubble is buoyancy-unstable [1,9,13]. Besides, it is illustrated that a more rapid reduction of the electrostatic pressure $P_e \sim 1/R^4$ compared with the Laplace pressure $P_L \sim 1/R$ as the size of the bubble increases [21]. All other things being equal, bubbles are more difficult to attain thermodynamic equilibrium. Despite we could not ascertain a specific range of bubble size due to the divergence of experimental conditions, it can be found that the charge stabilization model is more applicable to nano-sized bubbles.

Next, we explore quantitatively the coupling action of surface tension and surface charge tuned by the ionic surfactants on the stable equilibrium state of bulk nanobubbles. Intuitively, the addition of ionic surfactants introduces changes in three factors: the surface tension of the gas–liquid interface (σ), the surface charge (zeta potential ζ) on the bubble surface, and the ionic strength in solution (substantially Debye length κ^{-1}). As the concentration of surfactant in the solution increases, more surfactant ions can be adsorbed to the gas–liquid interface, further increasing the surface charge density, as shown in Fig. 7(a). For both SDS and CTAB cases, the relationship between the surface charge density of nanobubbles and the concentration of surfactant in solution can be fitted well by a power function. In the present experiments, the surface charge density of negatively charged nanobubbles suspended in anionic surfactant solution SDS is at least twice as high as that of positively charged nanobubbles at similar magnitudes of zeta potentials. This suggests that even at high Zeta potentials (~80 mV), the surface of the positively charged nanobubbles still seems to have enough space to allow the adsorption of surface charges, either from CTAB surfactant ions or from other ions, such as OH^-. However, based on the experimental results shown in Fig. 4(e~h), the stability state and surface potential of the positively charged nanobubbles did not change. This validates our conclusion that, at surfactant concentrations close to the CMC, surfactant ions or surface charges have reached the saturation adsorption limit on the bubble surface. A state of homeostasis is expected and the net accumulation of charged ions on the surface of the nanobubble ceases. Whereas CTAB surfactant ions occupy a larger cross-sectional area than the SDS surfactant ions do.

Having formulated a consistent model, we then present quantitative predictions by taking negatively charged nanobubbles (in SDS solutions) as an example. Once the new equilibrium state is reached, the absorbed surface charges generate an electric field that collocates with the subsequent build-up of the nanobubble's electric double layer. To predict nanobubble stability, one needs to relate the equilibrium size to the Zeta potential. Fig. 7(b) gives the Zeta potential as a function of equilibrium radius for nanobubbles in a thermodynamic stable state. In the calculation, the interfacial tension dependence on surfactant concentration is referred to Fig. 1(c). Indeed, the stable equilibrium radius of nanobubbles ($R < 500$ nm) is significantly dependent on the Zeta potential, while that of the microbubbles ($R > 500$ nm) shows a weak Zeta potential dependence. As expected, when the amount of surfactant added is high enough, e.g., close to the CMC, nanobubbles can be naturally stabilized under the combined action of surface charge and surface tension. This also theoretically explains the experimental results shown in Fig. 4(e~h). Nonetheless, for the cases with low surfactant concentrations, the magnitude of the Zeta potential required for a nanobubble of the same size to remain stable increases dramatically. Such high Zeta potentials (~100 mV) were not observed in the experiments, and thus the stability of these nanobubbles cannot be covered by the present model. More efforts are needed to rationalize the stability of these nanobubbles, such as introducing other types of non-electrostatic repulsive interactions (as discussed in recent papers [10,13,58]).

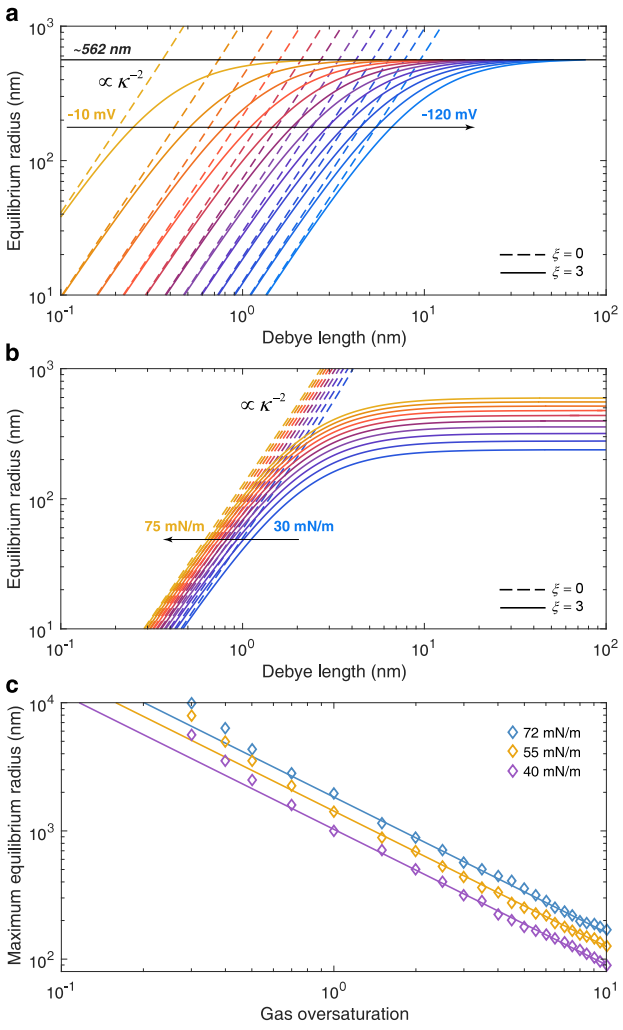

Fig. 8. Calculated stable equilibrium size of bulk nanobubbles. (a) Stable equilibrium radii of bulk nanobubbles under the spectrum of Debye lengths of $0.1 < \kappa^{-1} < 100$ nm, for various Zeta potential, $\zeta = -10 \sim -120$ mV, and for two gas supersaturations $\xi = 0, 3$. (b) Stable equilibrium radii of bulk nanobubbles under the spectrum of Debye lengths of $0.1 < \kappa^{-1} < 100$ nm, for various interfacial tension, $\gamma = 30 \sim 75$ mN/m, and for two gas supersaturations $\xi = 0, 3$. The Zeta potential is fixed at −50 mV. (c) Maximum equilibrium radius of bulk nanobubbles with $\gamma = 40, 55, 72$ as a function of the gas supersaturation. These solid lines represent the best fit.

We then broaden the parametric space of the study, essentially, decoupling the effects of surface charge and surface tension on the nanobubble stable state. Fig. 8(a) shows how the stable equilibrium radius of individual nanobubbles R depends on Debye length κ^{-1}, for a variety of Zeta potentials ranging from −10 mV to −120 mV. Here two values of gas supersaturation, $\xi = 0, 3$, are considered. The dependence of equilibrium radius on Debye length exhibits consistent behavior, e.g., for $\xi = 0$, $R \propto \kappa^{-2}$. The κ^{-1} dependence of equilibrium radius represents the electrolyte concentration dependence of equilibrium radius. When suspended in the solution with high ionic strength, the surface potential required for nanobubbles to maintain stable equilibrium is relatively low. However, as ξ increases to 3, the dependence of equilibrium radius on κ^{-1} shows contrasting behaviors at the spectrum's extremes. With increasing κ^{-1}, the curves deviate from the power law $R \propto \kappa^{-2}$, and the equilibrium radius, ultimately, becomes κ^{-1} independent in the solutions with low ionic strength. The finite supersaturation seems to set up an equilibrium size limit. Interestingly, all curves collapse to the same plateau value (~562 nm),

indicating Zeta-potential independence. Based on the abovementioned procedures, we obtain the equilibrium radius versus the Debye length as the interfacial tension is changed from $30 < \gamma < 75$ mN/m, as shown in Fig. 8(b). As the interfacial tension increases, a higher concentration of screening electrolytes (lower Debye length) is required to stabilize the nanobubbles with the curve shifting towards the left. Moreover, the maximum possible equilibrium radius determined by finite supersaturation ($\xi = 3$) depends significantly on the interfacial tension. In Fig. 8(c), the maximum equilibrium radii are plotted for $\gamma = 40, 55, 72$, as the gas supersaturation is varied from 0 to 10. It is apparent that increasing the degree of supersaturation and lowering the interfacial tension notably narrow the size range of nanobubble stabilization. In our experiments, the upper limit of the size of the prepared nanobubbles is about 300 nm, which corresponds to the expected gas supersaturation of the solution of 3~5. Supersaturation is usually required for nanobubble nucleation, however once nucleated, they remain stable even in macroscopically undersaturated solutions. This prediction appears to contradict the results of the experiment, in which the supersaturation ξ of the solution falls between 0~1.

Not surprisingly, the stability of bulk nanobubbles is much more comprehensive evaluation, towards an atomic-scale understanding, should be taken into consideration. The fact, that the air–water interface is a structured environment in which the hydrogen-bond network of water molecules is interrupted and displays specific orientational distribution, has been well established. This fascinating structure of interfacial water as distinct from the bulk seems to have two important consequences. One is that, the physicochemical properties parameters of the interfacial layer, such as relative permittivity and density, should be modified. The other consequence is that, the interaction of air–water interface polarization [10], arising from the preferred water-molecule orientations, should be considered seriously as it may also exert a radially outward pressure contribution. Evidently, both are challenging tasks, and there is still a long way to go in rationalizing the stability of bulk nanobubbles.

4. Conclusions

To summarize, we have probed experimentally the characteristics of bulk nanobubbles generated in three representative surfactant solutions (anionic, cationic, and nonionic) over a wide range of concentrations. Experimental results show that bulk nanobubbles can nucleate and remain somewhat stable in all three surfactant solutions, featuring a similar range of size distribution (<~500 nm) and almost uniform peak size (~125 nm). The striking difference in the effects of ionic and nonionic surfactants on the properties of bulk nanobubbles reveals the dominant role of the surface charge. The origin of these surface charges could be ascribed to the adsorption of charge carriers, surfactants, and ions, at the gas–liquid interface with limited adsorption sites.

Then we explored the reported long-term stability of bulk nanobubbles over 48 h and found that the magnitude of Zeta potential, arising from the accumulation of net charges, whether positive or negative, is responsible for the stability of bulk nanobubbles. The uncharged or slightly charged nanobubbles lose their stability and disappear over time scale typically much longer than predicted, either by collapsing naturally or by coalescing with nearby bubbles. In particular, the stability of those nanobubbles whose surfaces do not reach a saturated level of surfactant should also take into account the effects of negative charges that are continuously adsorbed to the surface during storage. Regardless of the initial sign, the nanobubble surface potential would become more and more negative over time. However, in contrast to our previous study [30], it was found that the Zeta potential originating from ion adsorption is more robust than that originating from surfactant ion adsorption. We stress that, the role of surface tension in nanobubble stabilization remains obscure, at least in this study it appears to have a limited effect. As amphiphilic molecule, it may simply play a role in nanobubble nucleation, for example by reducing the surface tension of the solution, in agreement with a recent study [59]. Further, based on classic DLVO theory, we evaluate the kinetic stability of multiple nanobubbles suspended in different concentrations of surfactants. A positive energy barrier ranging from 20 k_BT to 250 k_BT against collapse or coalescence is found for SDS-stabilized nanobubbles, while the energy barrier for CTAB-stabilized nanobubbles returns to positive only in high-concentration surfactant solutions.

Finally, through the theoretical analysis of the charge-stabilization model, we quantitatively reveal the dependence of the surface charge density on the bulk surfactant concentration. At surfactant concentrations close to the CMC, a state of homeostasis is expected and the net accumulation of charges (positive or negative) on the surface of the nanobubble ceases. We demonstrate that the stable equilibrium size of the nanobubbles is extremely sensitive to the ionic environment of the solution. There is an upper limit of equilibrium radius for stably surviving nanobubbles, which depends on both the interfacial tension and the supersaturation of the solution, and weakly on the surface potential. The present theoretical understanding posits that, both the surface charging/lowering interfacial tension (sufficiently) and supersaturation must be present for nanobubbles to remain stable but cannot rationalize why they exist under ambient conditions (exactly saturated or undersaturated water), e.g., without enough surfactant added.

Although the results reported herein are highly encouraging, other relevant issues are still worth pursuing. More comprehensive and well-designed experiments should be conducted to explore the underlying mechanism, especially the structure of the gas–liquid interface, for stable bulk nanobubbles. As for individual ones, molecular dynamic simulations illuminate qualitative insights about how nanobubble behaves under experimental conditions, and thus provide more information to understand the bubble dynamics at the nano-scale.

CRediT authorship contribution statement

Xiaotong Ma: Conceptualization of this study, Data curation, Writing – original draft, Visualization, Methodology, Software. **Mingbo Li:** Conceptualization of this study, Writing – original draft, Software, Visualization, Data curation, Validation, Supervision. **Xuefei Xu:** Writing – review & editing, Methodology. **Chao Sun:** Supervision, Writing – review & editing, Funding acquisition, Project administration.

Declaration of competing interest

The authors declare that they have no known competing financial interests or personal relationships that could have appeared to influence the work reported in this paper.

Data availability

No data was used for the research described in the article.

Acknowledgments

This work was financially supported by the National Natural Science Foundation of China under Grant Nos. 11988102, 91852202 and 12202244, and Tencent Foundation through the XPLORER PRIZE.

Appendix A. Supplementary data

Supplementary material related to this article can be found online at https://doi.org/10.1016/j.apsusc.2022.155232. Supplementary data associated with this article can be found in a separate file.

References

[1] M. Alheshibri, J. Qian, M. Jehannin, V.S. Craig, A history of nanobubbles, Langmuir 32 (43) (2016) 11086–11100.
[2] A. Agarwal, W.J. Ng, Y. Liu, Principle and applications of microbubble and nanobubble technology for water treatment, Chemosphere 84 (9) (2011) 1175–1180.
[3] J. Zhu, H. An, M. Alheshibri, L. Liu, P.M. Terpstra, G. Liu, V.S. Craig, Cleaning with bulk nanobubbles, Langmuir 32 (43) (2016) 11203–11211.
[4] T. Temesgen, T.T. Bui, M. Han, T.-i. Kim, H. Park, Micro and nanobubble technologies as a new horizon for water-treatment techniques: A review, Adv. Colloid Interface Sci. 246 (2017) 40–51.
[5] A. Azevedo, H. Oliveira, J. Rubio, Bulk nanobubbles in the mineral and environmental areas: Updating research and applications, Adv. Colloid Interface Sci. 271 (2019) 101992.
[6] E.P. Favvas, G.Z. Kyzas, E.K. Efthimiadou, A.C. Mitropoulos, Bulk nanobubbles, generation methods and potential applications, Curr. Opin. Colloid Interface Sci. 54 (2021) 101455.
[7] K. Yuan, L. Zhou, J. Wang, Z. Geng, J. Qi, X. Wang, L. Zhang, J. Hu, Formation of bulk nanobubbles induced by accelerated electrons irradiation: Dependences on dose rates and doses of irradiation, Langmuir (2022).
[8] P.S. Epstein, M.S. Plesset, On the stability of gas bubbles in liquid-gas solutions, J. Chem. Phys. 18 (11) (1950) 1505–1509.
[9] N. Nirmalkar, A. Pacek, M. Barigou, On the existence and stability of bulk nanobubbles, Langmuir 34 (37) (2018) 10964–10973.
[10] M.R. Ghaani, P.G. Kusalik, N.J. English, Massive generation of metastable bulk nanobubbles in water by external electric fields, Sci. Adv. 6 (14) (2020) eaaz0094.
[11] K. Yasui, T. Tuziuti, W. Kanematsu, K. Kato, Dynamic equilibrium model for a bulk nanobubble and a microbubble partly covered with hydrophobic material, Langmuir 32 (43) (2016) 11101–11110.
[12] N. Taccoen, F. Lequeux, D.Z. Gunes, C.N. Baroud, Probing the mechanical strength of an armored bubble and its implication to particle-stabilized foams, Phys. Rev. X 6 (1) (2016) 011010.
[13] B.H. Tan, H. An, C.-D. Ohl, Stability of surface and bulk nanobubbles, Curr. Opin. Colloid Interface Sci. (2021) 101428.
[14] L. Zhang, H. Chen, Z. Li, H. Fang, J. Hu, Long lifetime of nanobubbles due to high inner density, Sci. China G 51 (2) (2008) 219–224.
[15] P. Attard, The stability of nanobubbles, Eur. Phys. J. Spec. Top. 223 (5) (2014) 1–22.
[16] S. Wang, L. Zhou, X. Wang, J. Hu, P. Li, G. Lin, Y. Gao, L. Zhang, C. Wang, Collective dynamics of bulk nanobubbles with size-dependent surface tension, Langmuir 37 (26) (2021) 7986–7994.
[17] N. Bunkin, F. Bunkin, Bubbstons: stable microscopic gas bubbles in very dilute electrolytic solutions, Sov. Phys.—JETP 74 (2) (1992) 271–276.
[18] M. Chaplin, Theory versus experiment. what is the charge at the surface of water, Multidiscip. Res. J. 2 (2009) 1–28.
[19] N. Nirmalkar, A. Pacek, M. Barigou, Interpreting the interfacial and colloidal stability of bulk nanobubbles, Soft Matter 14 (47) (2018) 9643–9656.
[20] J.N. Meegoda, S.A. Hewage, J.H. Batagoda, Application of the diffused double layer theory to nanobubbles, Langmuir 35 (37) (2019) 12100–12112.
[21] B.H. Tan, H. An, C.-D. Ohl, How bulk nanobubbles might survive, Phys. Rev. Lett. 124 (13) (2020) 134503.
[22] H. Zhang, Z. Guo, X. Zhang, Surface enrichment of ions leads to the stability of bulk nanobubbles, Soft Matter 16 (23) (2020) 5470–5477.
[23] J.-Y. Kim, M.-G. Song, J.-D. Kim, Zeta potential of nanobubbles generated by ultrasonication in aqueous alkyl polyglycoside solutions, J. Colloid Interface Sci. 223 (2) (2000) 285–291.
[24] A. Gray-Weale, J.K. Beattie, An explanation for the charge on water's surface, Phys. Chem. Chem. Phys. 11 (46) (2009) 10994–11005.
[25] R. Vacha, O. Marsalek, A.P. Willard, D.J. Bonthuis, R.R. Netz, P. Jungwirth, Charge transfer between water molecules as the possible origin of the observed charging at the surface of pure water, J. Phys. Chem. Lett. 3 (1) (2012) 107–111.
[26] D.V. Matyushov, Electrophoretic mobility without charge driven by polarisation of the nanoparticle–water interface, Mol. Phys. 112 (15) (2014) 2029–2039.
[27] Y. Uematsu, D.J. Bonthuis, R.R. Netz, Charged surface-active impurities at nanomolar concentration induce jones–ray effect, J. Phys. Chem. Lett. 9 (1) (2018) 189–193.
[28] M. Sparnaay, Corrections of the theory of the flat diffuse double layer, Recl. Trav. Chim. Pays-Bas 77 (9) (1958) 872–888.
[29] M. Manciu, E. Ruckenstein, Ions near the air/water interface: I. compatibility of zeta potential and surface tension experiments, Colloids Surf. A 400 (2012) 27–35.
[30] X. Ma, M. Li, P. Pfeiffer, J. Eisener, C.-D. Ohl, C. Sun, Ion adsorption stabilizes bulk nanobubbles, J. Colloid Interface Sci. 606 (2022) 1380–1394.
[31] U. Zoller, Handbook of Detergents, Part E: Applications, CRC Press, 2008.
[32] P. Raffa, A.A. Broekhuis, F. Picchioni, Polymeric surfactants for enhanced oil recovery: A review, J. Pet. Sci. Eng. 145 (2016) 723–733.
[33] W. Liu, W. Liu, X. Wang, D. Wei, B. Wang, Utilization of novel surfactant n-dodecyl-isopropanolamine as collector for efficient separation of quartz from hematite, Sep. Purif. Technol. 162 (2016) 188–194.
[34] H.-J. Butt, K. Graf, M. Kappl, Physics and Chemistry of Interfaces, John Wiley & Sons, 2013.
[35] E. Dressaire, R. Bee, D.C. Bell, A. Lips, H.A. Stone, Interfacial polygonal nanopatterning of stable microbubbles, Science 320 (5880) (2008) 1198–1201.
[36] S.-H. Cho, J.-Y. Kim, J.-H. Chun, J.-D. Kim, Ultrasonic formation of nanobubbles and their zeta-potentials in aqueous electrolyte and surfactant solutions, Colloids Surf. A 269 (1–3) (2005) 28–34.
[37] M. Parhizkar, M. Edirisinghe, E. Stride, The effect of surfactant type and concentration on the size and stability of microbubbles produced in a capillary embedded t-junction device, Rsc Adv. 5 (14) (2015) 10751–10762.
[38] T.T. Bui, D.C. Nguyen, M. Han, Average size and zeta potential of nanobubbles in different reagent solutions, J. Nanopart. Res. 21 (8) (2019) 1–11.
[39] M. Li, X. Ma, J. Eisener, P. Pfeiffer, C.-D. Ohl, C. Sun, How bulk nanobubbles are stable over a wide range of temperatures, J. Colloid Interface Sci. 596 (2021) 184–198.
[40] J. Schindelin, I. Arganda-Carreras, E. Frise, V. Kaynig, M. Longair, T. Pietzsch, S. Preibisch, C. Rueden, S. Saalfeld, B. Schmid, et al., Fiji: an open-source platform for biological-image analysis, Nature Methods 9 (7) (2012) 676–682.
[41] T. Wagner, H.-G. Lipinski, M. Wiemann, Dark field nanoparticle tracking analysis for size characterization of plasmonic and non-plasmonic particles, J. Nanopart. Res. 16 (5) (2014) 1–10.
[42] M. Alheshibri, A. Al Baroot, L. Shui, M. Zhang, Nanobubbles and nanoparticles, Curr. Opin. Colloid Interface Sci. 55 (2021) 101470.
[43] W. Xiao, X. Wang, L. Zhou, W. Zhou, J. Wang, W. Qin, G. Qiu, J. Hu, L. Zhang, Influence of mixing and nanosolids on the formation of nanobubbles, J. Phys. Chem. B 123 (1) (2018) 317–323.
[44] V. Olszok, J. Rivas-Botero, A. Wollmann, B. Benker, A.P. Weber, Particle-induced nanobubble generation for material-selective nanoparticle flotation, Colloids Surf. A 592 (2020) 124576.
[45] M. Zhang, J.R. Seddon, Nanobubble–nanoparticle interactions in bulk solutions, Langmuir 32 (43) (2016) 11280–11286.
[46] M. Alheshibri, V.S. Craig, Armoured nanobubbles; ultrasound contrast agents under pressure, J. Colloid Interface Sci. 537 (2019) 123–131.
[47] A.J. Jadhav, M. Barigou, Bulk nanobubbles or not nanobubbles: That is the question, Langmuir 36 (7) (2020) 1699–1708.
[48] Z. Huang, M. Su, Q. Yang, Z. Li, S. Chen, Y. Li, X. Zhou, F. Li, Y. Song, A general patterning approach by manipulating the evolution of two-dimensional liquid foams, Nature Commun. 8 (1) (2017) 1–9.
[49] X. Zheng, J. Jang, Hydraulic properties of porous media saturated with nanoparticle-stabilized air–water foam, Sustainability 8 (12) (2016) 1317.
[50] N.F. Bunkin, A.V. Shkirin, N.V. Penkov, M.V. Goltayev, P.S. Ignatiev, S.V. Gudkov, A.Y. Izmailov, Effect of gas type and its pressure on nanobubble generation, Front. Chem. 9 (2021) 630074.
[51] Y. Zhou, Z. Han, C. He, Q. Feng, K. Wang, Y. Wang, N. Luo, G. Dodbiba, Y. Wei, A. Otsuki, et al., Long-term stability of different kinds of gas nanobubbles in deionized and salt water, Materials 14 (7) (2021) 1808.
[52] A.K.A. Ahmed, X. Shi, L. Hua, L. Manzueta, W. Qing, T. Marhaba, W. Zhang, Influences of air, oxygen, nitrogen, and carbon dioxide nanobubbles on seed germination and plant growth, J. Agricult. Food Chem. 66 (20) (2018) 5117–5124.
[53] W.J. Galloway, An experimental study of acoustically induced cavitation in liquids, J. Acoust. Soc. Am. 26 (5) (1954) 849–857.
[54] J.N. Israelachvili, Intermolecular and Surface Forces, Academic Press, 2011.
[55] J. Gregory, Approximate expressions for retarded van der waals interaction, J. Colloid Interface Sci. 83 (1) (1981) 138–145.
[56] E.M. Lifshitz, M. Hamermesh, et al., The theory of molecular attractive forces between solids, in: Perspectives in Theoretical Physics, Elsevier, 1992, pp. 329–349.
[57] K. Makino, H. Ohshima, Electrophoretic mobility of a colloidal particle with constant surface charge density, Langmuir 26 (23) (2010) 18016–18019.
[58] L. Zhou, S. Wang, L. Zhang, J. Hu, Generation and stability of bulk nanobubbles: A review and perspective, Curr. Opin. Colloid Interface Sci. 53 (2021) 101439.
[59] J.I. Lee, J.-M. Kim, Role of anionic surfactant in the generation of bulk nanobubbles by ultrasonication, Colloid Interface Sci. Commun. 46 (2022) 100578.